

Cite this article as: Peng Zhaowei, Li Weizhou, Peng Chengzhang. Microstructure and Corrosion Resistance of Electrodeposited Ni-Fe-Co Alloy Coatings[J]. Rare Metal Materials and Engineering, 2023, 52(05): 1593-1602.

ARTICLE

Microstructure and Corrosion Resistance of Electrodeposited Ni-Fe-Co Alloy Coatings

Peng Zhaowei^{1,2,3}, Li Weizhou^{1,3}, Peng Chengzhang⁴

¹School of Resources, Environment and Materials, Guangxi University, Nanning 530004, China; ²School of Chemistry and Chemical Engineering, Guangxi University, Nanning 530004, China; ³Guangxi Key Laboratory of Processing for Non-Ferrous Metals and Featured Materials, Guangxi University, Nanning 530004, China; ⁴School of Mechanical Engineering, Hunan University of Science and Technology, Xiangtan 411201, China

Abstract: Ni-Fe-Co alloy coatings were obtained on mild steel substrates by electrodeposition from stable acidic citrate solution. The effects of plating conditions and cobalt content on the coating performance were investigated, and the optimal electrodeposition process parameters were obtained. The alloy coatings were investigated by scanning electron microscope, energy dispersive spectrometer, electrochemical impedance spectrum, polarization curve, and digital microhardness meter. Results show that the suitable processing parameters are 10 A/dm², 45 °C, and triammonium citrate of 10 g/L. The cobalt content of Ni-Fe-Co alloy coatings is increased linearly with increasing the cobalt ion content. The coatings have simple face-centered cubic solid solution structure. With increasing the cobalt content in the coating, the corrosion resistance and microhardness of coatings are increased firstly and then decreased. The Ni-Fe-13.51Co (wt%) coating exhibits the remarkable corrosion resistance: the charge transfer resistance is 3031 Ω·cm², and the corrosion current density is 5.754×10⁻⁶ A/cm².

Key words: electrodeposition; Ni-Fe-Co alloy coatings; microhardness; corrosion

Surface modification, particularly coating, plays a crucial role in enhancement of mechanical properties, tribological performance, and corrosion behavior of engineering components^[1-4]. Laser surface engineering, plasma spraying^[5], physical and chemical vapor deposition, and electrochemical treatment^[6-7] are commonly used surface modification techniques^[8]. Electrodeposition is a widely used coating preparation method due to its advantages of simple process, small raw material loss, low energy consumption, scalability, and versatility^[9].

Ni-Fe alloy coating has remarkable electrocatalytic property^[10], magnetic property^[11], and mechanical property^[12], thereby attracting much attention^[13]. Ni-Fe alloy is usually used as catalysis for hydrogen evolution reaction^[14], oxygen evolution reaction^[15], and CO₂ reduction reaction^[16] due to its excellent electronic structure. Besides, Ni-Fe alloy can be applied in the fabrication of magnetic resonance imaging/sensors^[17] and semiconductors^[18] owing to its outstanding soft

magnetic properties. Ni-Fe alloy coating has been extensively used to protect steel in the replacement of pure Ni coating^[19-20], because it can simultaneously reduce the production cost and maintain the good performance (high mechanical strength, good ductility, and excellent corrosion resistance). Li et al^[21] prepared the Ni-Fe alloy coating on Fe plate via electrodeposition method, and found that due to the nanocrystalline and compact surface, the Ni-Fe alloy coating has good corrosion resistance. Cobalt can be added into Ni-Fe alloy to form the ternary Ni-Fe-Co alloy, which has higher magnetism and lower oxidation rate, compared with those of Ni-Fe or Ni-Co alloys^[22-23]. Liu et al^[24] prepared soft Co₅₂Fe₂₆Ni₂₂ alloy films with high moment by electrodeposition from a sulfate-based electrolyte without additives, and found that the corrosion rate of the model alloy with high Co content is slow.

The codeposition of Ni-Fe alloy coating via electroplating is feasible, and the composition of deposited Ni-Fe alloy coatings can be easily controlled by adjusting the metal cation

Received date: July 31, 2022

Foundation item: Major Science and Technology Projects in Guangxi (AA18118030, AA17204100); Hunan Provincial Natural Science Foundation of China (19A177)
Corresponding author: Li Weizhou, Ph. D., Professor, School of Resources, Environment and Materials, Guangxi University, Nanning 530004, P. R. China, Tel: 0086-771-3270152, E-mail: wz-li@hotmail.com

Copyright © 2023, Northwest Institute for Nonferrous Metal Research. Published by Science Press. All rights reserved.

(Ni²⁺ and Fe²⁺) contents in the electroplating solution. In this research, the Ni-Fe-Co alloy coatings were prepared by electrodeposition on mild steel substrates from acidic sulphate-citrate baths. The suitable processing parameters of electrodeposition of Ni-Fe-Co alloy coating were discussed. Different bath components were used to prepare different alloy coatings. The coatings were characterized and the morphology and microhardness of Ni-Fe-Co alloy coatings were studied. Finally, the corrosion behavior of the coatings was investigated by electrochemical measurements^[25-26], and the relationship between corrosion resistance and the microstructure/surface morphology of the coatings was studied.

1 Experiment

Five plating baths with different CoSO₄ contents were prepared at 25 °C. NiSO₄ content was kept at 100 g/L and FeSO₄ content was kept at 10 g/L in all the baths. The CoSO₄ content varied from 0 g/L to 12 g/L. Bath A, Bath B, Bath C, Bath D, and Bath E contained 3, 6, 9, 12, and 0 g/L CoSO₄, respectively. The trisodium citrate (20 g/L) and sodium citrate (20 g/L) were added as the complexing agent. The pH value of the baths was adjusted to 4 by sulphuric acid solution. All the used chemicals were at laboratory grade.

The mild steel substrates (20 mm×10 mm×2 mm) were used as the cathode and the pure nickel strips were used as anode. The specimens were ground by 600# SiC paper. Before experiment, the specimens were soaked in the dilute hydrochloric acid solution for 30 s to remove the oxide film and to form a rough surface. This treatment could enhance the adhesion between the substrate and deposition layer. After that, the specimens were ultrasonically cleaned in alcohol and distilled water. The pre-treated specimens were electrodeposited by a self-made electrodeposition setup, as shown in Fig.1. The electrodeposition setup consisted of a direct-current (DC) power supply, an electrodeposition tank, a nickel plate, some clamps, and a water bath. The distance between anode and cathode was 5 cm. The electrodeposition experiments were conducted in galvanostatic mode at current density of 4–12 A/dm² by DC power supply (DH1716-5D). The deposition duration was 2 h, and the deposition temperature was 35–55 °C. Triammonium citrate content was 0–20 g/L. The electrodeposition experiment was repeated at least three times.

The phase composition of Ni-Fe-Co alloy coatings was characterized by X-ray diffraction (XRD, Rigaku D/MAX) by Cu K α radiation (0.154 18 nm) at 40 kV and 40 mA with $2\theta=$

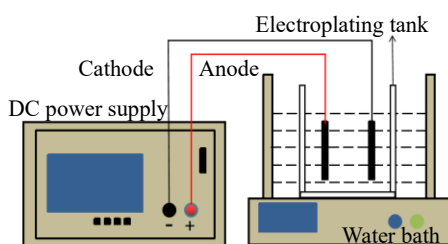


Fig.1 Schematic diagram of electrodeposition setup

20°–90° and scanning rate of 6°/min. The scanning electron microscope (SEM, SU-8020) was used to observe the coating surface morphology and microstructure. Energy dispersive spectrometer (EDS, X-MAX 80) was used to analyze the element composition of the coatings. The microhardness of alloy coatings was measured by a microhardness tester (HXS-1000A) with load of 2 N and retention time of 5 s.

The corrosion resistance of Ni-Fe-Co alloy coatings was evaluated through electrochemical impedance spectroscopy (EIS) and potentiodynamic polarization scanning curves. EIS measurements were conducted by an electrochemical workstation (CHI760E) in 3.5wt% NaCl solution. The saturated calomel electrode and platinum foil were used as the reference and counter electrodes, respectively. During EIS tests, the exposed area was 1 cm², and the specimens were immersed in NaCl solution at room temperature. Electrochemical impedance measurement was performed at open circuit potential (OCP). The wave amplitude was 5 mV and the frequency was 10⁴–10⁻¹ Hz. EIS analysis was performed by the Zview software. The corrosion behavior of the specimens was evaluated by the potentiodynamic polarization scanning measurements in 3.5wt% NaCl solution at scanning rate of 0.01 V/s. The voltage was set as OCP \pm 1.5 V. Tafel extrapolation method was used to calculate the corrosion potential (E_{corr}) and corrosion current density (I_{corr}) of the alloy coatings for the evaluation of corrosion resistance of the alloy coatings.

2 Results and Discussion

2.1 Bath characterization

Fig.2 shows the linear sweep voltammograms of cathodic potential-current behavior for Bath A, B, C, and D with scanning rate of 100 mV/s. Since the potential sweep is along the opposite direction of OCP direction, the mild steel electrode is cathodically polarized. It can be observed that the polarization curves shift towards the negative direction with increasing the CoSO₄ content. The higher the cobalt content, the larger the cathodic current^[25]. The voltammograms depict a slight increase in the cathodic current at about -0.6 V followed by a rapid increase at -0.98 V. The cathodic current reaches a peak value at about -1.37 V for Bath A, and it

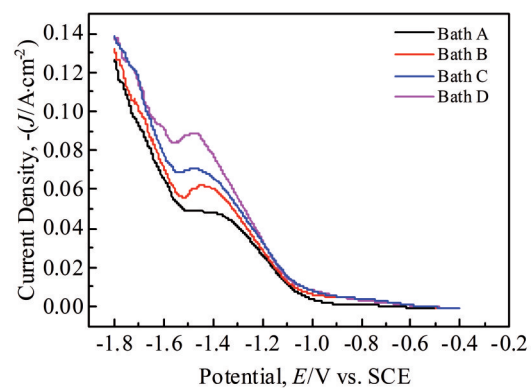


Fig.2 Influence of different content of cobalt sulfate on cathode polarization curves

reaches the peak value at about -1.46 V for Bath B, Bath C, and Bath D. The current starts to decrease with decreasing the potential from -1.46 V to -1.57 V. At about -1.57 V, the current starts to increase again. The two humps in the voltammograms are considered as the two-step discharge of complexed Co^{2+} ions. The discharge mechanism at the cathode is as follows:



2.2 Impact of main processing parameters on coating composition

Fig. 3 shows the effect of current density on the surface morphology of Ni-Fe-Co alloy coatings. It can be seen that the

Ni-Fe-Co alloy coatings are relatively flat at current density of $4\text{--}10$ A/dm^2 . When the current density reaches 12 A/dm^2 , the coating exhibits a cellular structure and the brightness decreases slightly.

The relationships between the component contents of the Ni-Fe-Co alloy coatings and current density are shown in Fig. 4 (CoSO_4 content is fixed as 12 g/L in the bath). When the current density is lower than 8 A/dm^2 , the content of iron, cobalt, and nickel barely changes, and the cobalt and iron contents are higher than the Co^{2+} and Fe^{2+} contents. With increasing the current density, the iron and cobalt contents of Ni-Fe-Co alloy coatings are gradually decreased from $17.70\text{wt}\%$ and $21.27\text{wt}\%$ to $12.14\text{wt}\%$ and $14.99\text{wt}\%$,

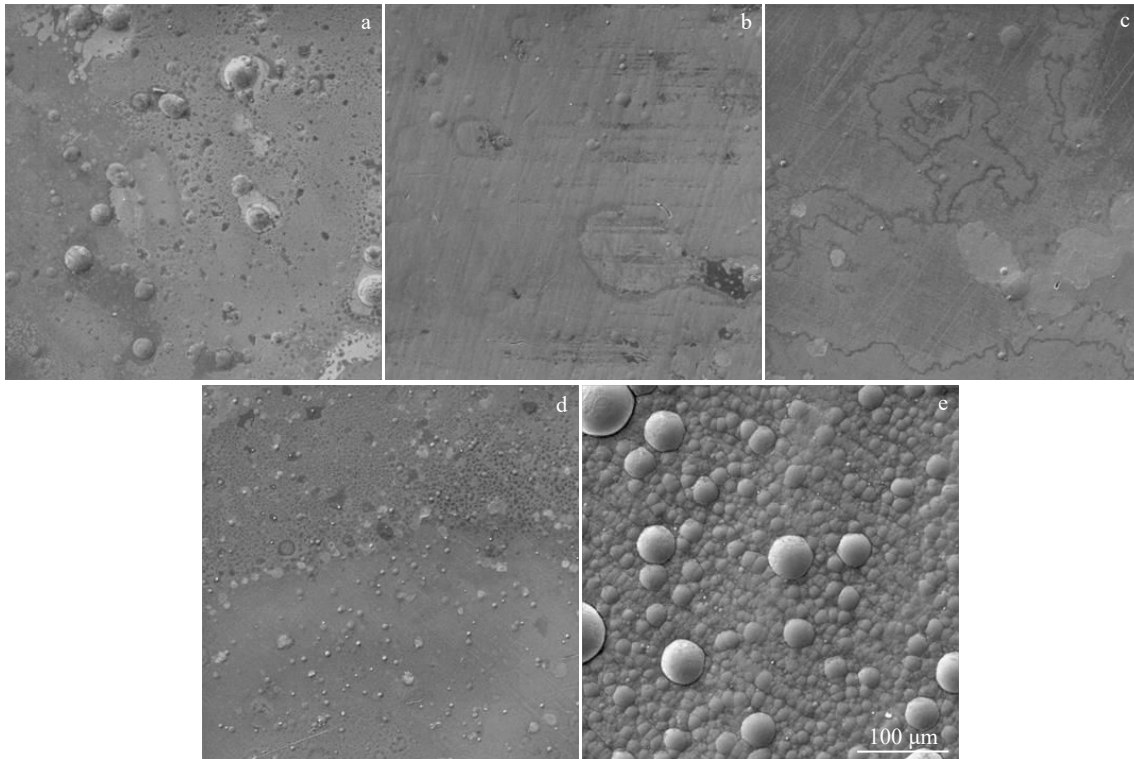


Fig. 3 Surface morphologies of Ni-Fe-Co alloy coatings after electrodeposition with different current densities: (a) 4 A/dm^2 , (b) 6 A/dm^2 , (c) 8 A/dm^2 , (d) 10 A/dm^2 , and (e) 12 A/dm^2

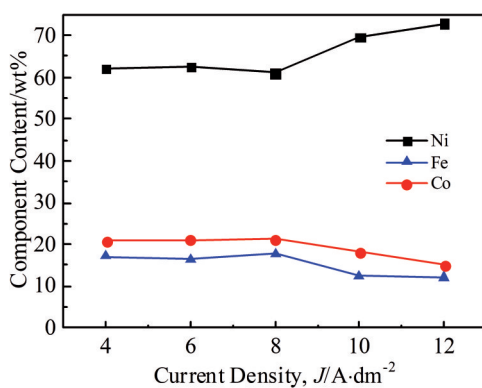


Fig. 4 Relationships between component contents in alloy coatings and current density

respectively. Meanwhile, the nickel content is increased from $61.03\text{wt}\%$ to $72.87\text{wt}\%$. These results are consistent with those in Ref. [24], verifying the dependence of alloy composition on current density.

Fig. 5 shows the effect of the electrodeposition temperature on the surface morphology of Ni-Fe-Co alloy coatings. The coating surface is smooth after electrodeposition at $35\text{--}55$ $^\circ\text{C}$. The relationships between the component contents of Ni-Fe-Co alloy coatings and the electrodeposition temperature are shown in Fig. 6 (CoSO_4 content is fixed as 12 g/L in the bath). With increasing the electrodeposition temperature, the iron and cobalt contents in the alloy coatings are increased simultaneously and the nickel content is decreased. When the electrodeposition temperature is 45 $^\circ\text{C}$, the iron and cobalt contents in the alloy coating are the highest and the nickel

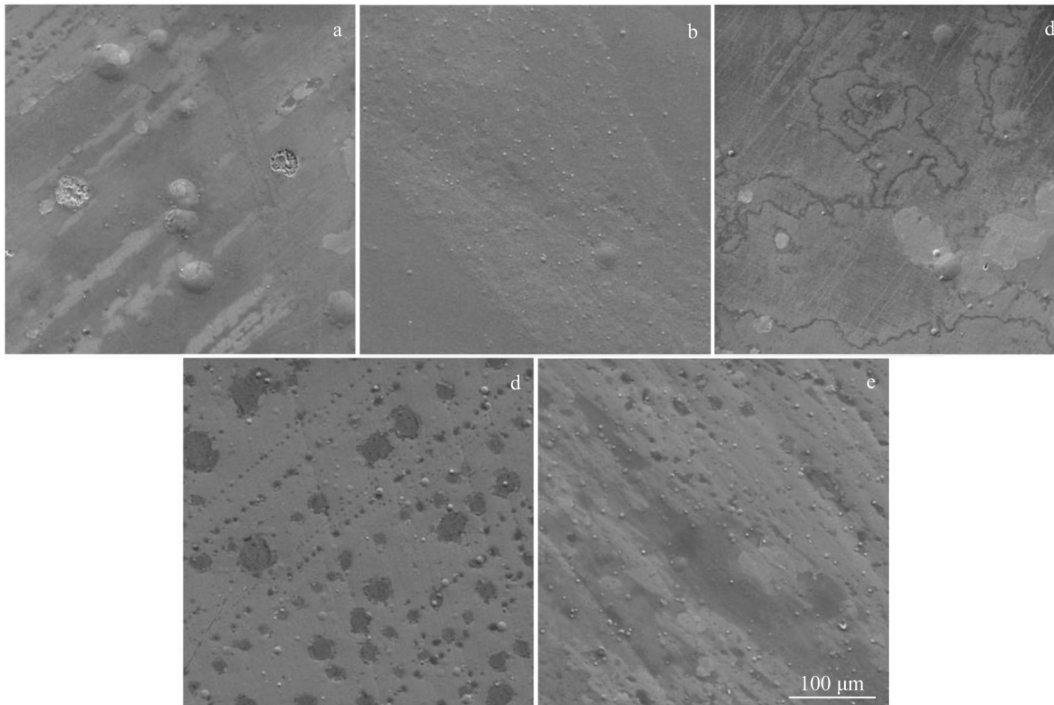


Fig.5 Surface morphologies of Ni-Fe-Co alloy coatings after electrodeposition at different temperatures: (a) 35 °C, (b) 40 °C, (c) 45 °C, (d) 50 °C, and (e) 55 °C

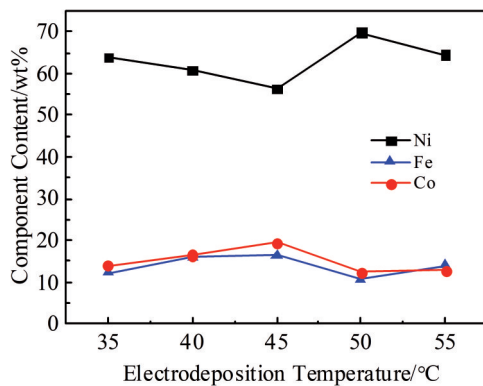


Fig.6 Relationships between component contents in alloy coatings and electrodeposition temperature

content is the lowest. With further increasing the electrodeposition temperature, the iron and cobalt contents in the alloy coatings are decreased, whereas the nickel content is increased.

Fig. 7 shows the surface morphologies of Ni-Fe-Co alloy coatings after electrodeposition with different triammonium citrate contents. The coating surfaces are relatively brighter when the triammonium citrate content is 5 and 10 g/L. With increasing the triammonium citrate content to 20 g/L, the adsorbent material can be observed. This is because when the triammonium citrate content is high, the iron and cobalt ions can easily form hydroxide on the cathode surface, which prevents the deposition of nickel ions and results in a large number of adsorbents on the surface. The relationships between the component contents of Ni-Fe-Co alloy coatings

and triammonium citrate content are shown in Fig. 8 (CoSO_4 content is fixed as 12 g/L in the bath). With increasing the triammonium citrate content in the electroplating solution, the content of iron and cobalt is decreased slightly, and the nickel content is slightly increased. When the triammonium citrate content exceeds 10 g/L, the content of iron and cobalt increases significantly, and the nickel content decreases.

2.3 Microstructure and properties of Ni-Fe-Co alloy coatings

Fig. 9 shows the appearances of Ni-Fe-Co alloy coatings with different Co contents, which are all bright and smooth. Fig. 10 shows the surface morphologies of Ni-Fe-Co alloy coatings. Combined with EDS analysis results, the average cobalt content of the alloy coatings prepared in Bath A, B, C, and D is 9.48wt%, 13.51wt%, 18.67wt%, and 23.38wt%, respectively. The effect of cobalt sulfate content in the electroplating solution on the cobalt content in the alloy coating is shown in Fig. 11. It can be seen that the cobalt content in alloy coating is increased linearly with increasing the cobalt sulfate content in the electroplating solution, indicating that the migration rate of Ni^{2+} , Fe^{2+} , and Co^{2+} to cathode and the discharge probability on cathode surface are basically the same in the electroplating solution. Therefore, the Ni-Fe-Co alloy coating can be obtained by controlling the ratio of $\text{Co}^{2+}/\text{Fe}^{2+}/\text{Ni}^{2+}$ in the electroplating solution.

As shown in Fig.10, the strip tissues and impurity appear on the surface of Ni-Fe-Co alloy coatings. According to Fig. 12, the iron, cobalt, and nickel contents of the strip tissue (point A in Fig. 10b) are 15.58wt% , 6.55wt% , and 71.65wt% , respectively; the iron, cobalt, and nickel contents of the

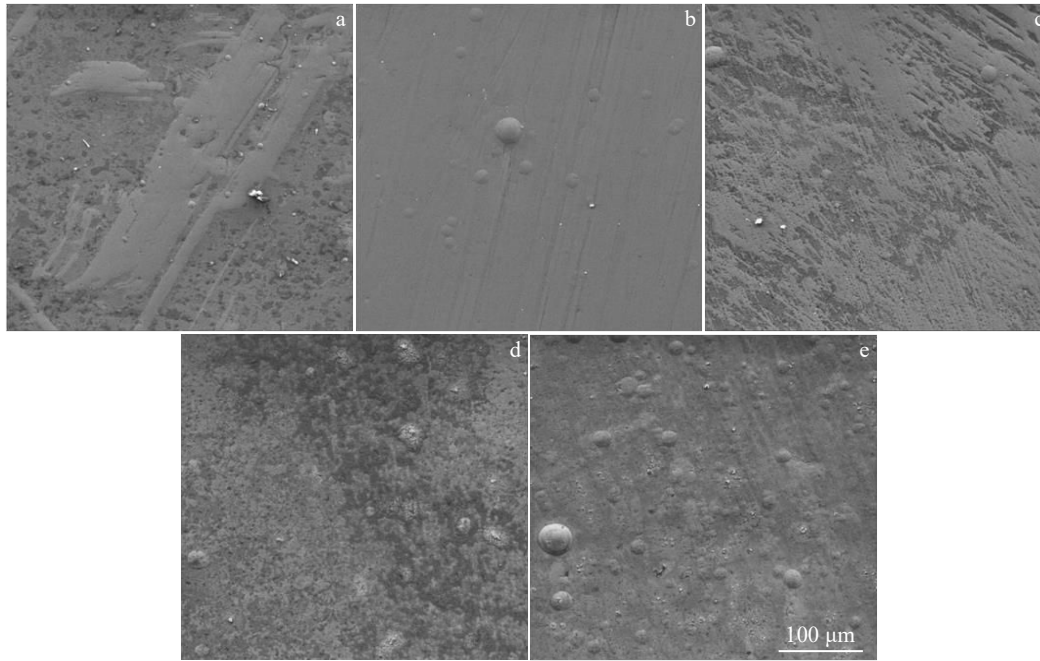


Fig.7 Surface morphologies of Ni-Fe-Co alloy coatings after electrodeposition with different triammonium citrate contents: (a) 0 g/L, (b) 5 g/L, (c) 10 g/L, (d) 15 g/L, and (e) 20 g/L

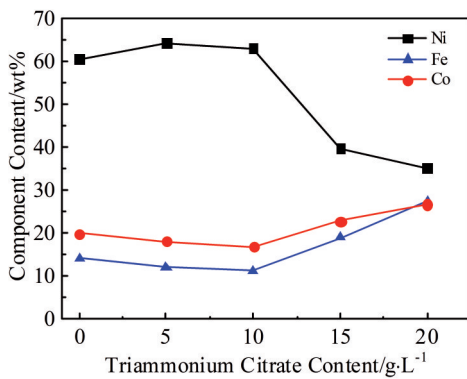


Fig.8 Relationships between component contents in alloy coatings and triammonium citrate content

coating (point B in Fig. 10b) are 14.69wt% , 8.86wt% , and 69.0wt% , respectively, suggesting the similar composition. The stripe tissue is caused by the lattice orientation generated by the deposition process. As shown in Fig. 13, the compact and homogenous alloy layer forms on the substrate. The

average thickness of the coating is about 26 μm, the adhesion between coating and substrate is satisfactory, and the Ni, Fe, and Co are evenly distributed in the alloy coatings.

Fig. 14 shows XRD spectra of different Ni-Fe-Co alloy coatings. It can be seen that the diffraction peaks of different alloy coatings are similar to each other. Since nickel, iron, and cobalt all show the complete solid solubility at room temperature, the single nickel-iron-cobalt phase forms in all specimens, indicating the non-existence of phase separation, which improves the corrosion resistance of the coating. Therefore, the possibility of current coupling is reduced, which may prevent the selective leaching of the anode phase.

Table 1 shows the microhardness of Ni-Fe-Co alloy coatings with different cobalt contents. It can be seen that when the cobalt content is 9.48wt%–18.67wt%, the coating microhardness is gradually increased from 6106.4 MPa to 6908.0 MPa (the maximum microhardness). With further increasing the cobalt content to 23.38wt% , the coating microhardness is decreased. The microhardness of Ni-Fe-Co coating is higher than that in Ref.[27], indicating that the Co

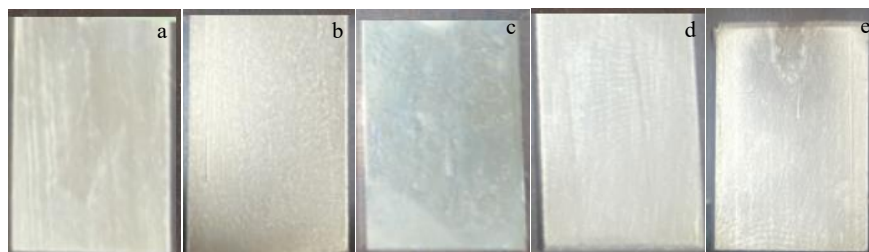


Fig.9 Appearances of Ni-Fe-Co alloy coatings with different Co contents: (a) 0wt%, (b) 9.48wt%, (c) 13.51wt%, (d) 18.67wt%, and (e) 23.38wt%

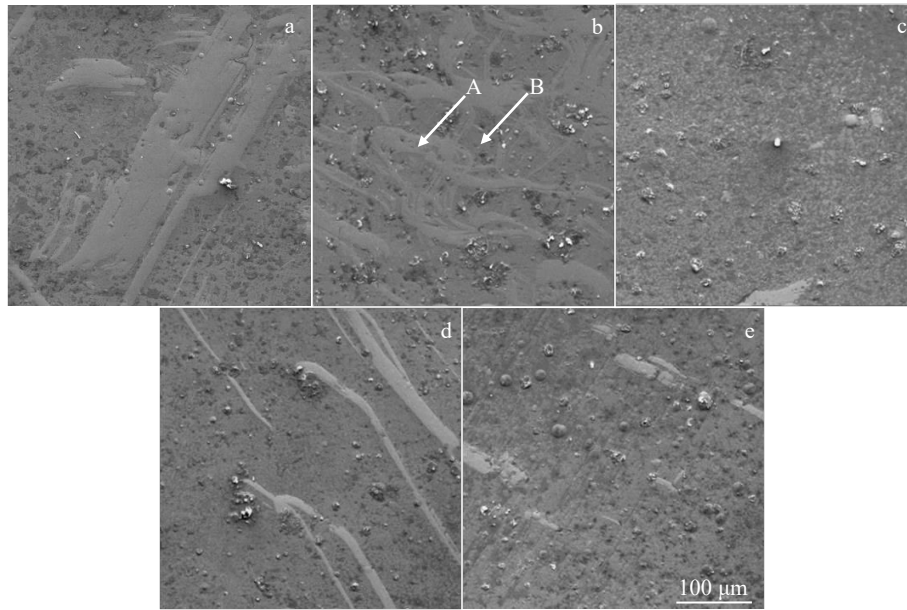


Fig.10 SEM surface morphologies of Ni-Fe-Co alloy coatings with different Co contents: (a) 0wt%, (b) 9.48wt%, (c) 13.51wt%, (d) 18.67wt%, and (e) 23.38wt%

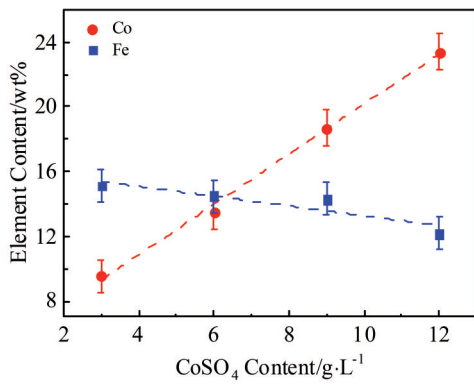


Fig.11 Effect of cobalt sulfate content on cobalt/iron content in Ni-Fe-Co alloy coatings

addition can enhance the alloy microhardness.

Fig.15a shows EIS spectra of Ni-Fe-Co alloy coatings with different cobalt contents. According to the Nyquist diagrams which consist of capacitive and inductive arcs, the radius of capacitive and inductive arcs of Ni-Fe-Co alloy coatings with different cobalt contents can be arranged in the decreasing order, as follows: 13.51wt%>9.48wt%>18.67wt%>23.38wt%>0wt%. The high frequency area of the Nyquist diagram mainly displays the interface information between the coating and the corrosive medium, and the low frequency area reflects the impedance information of the electrode surface. Fig. 16a shows the equivalent circuit of the Ni-Fe-Co alloy coatings with Co content of 0wt% – 18.67wt%. Fig. 16b shows the equivalent circuit of Ni-Fe-Co alloy coating with 23.38wt% Co. As shown in Fig. 16, R_s is the solution resistance, R_{ct} is the charge transfer resistance, and R_f is the resistance of the deposited coating. Due to the dispersion effect of the corroded surface, the constant phase element C_{dl} produced by the

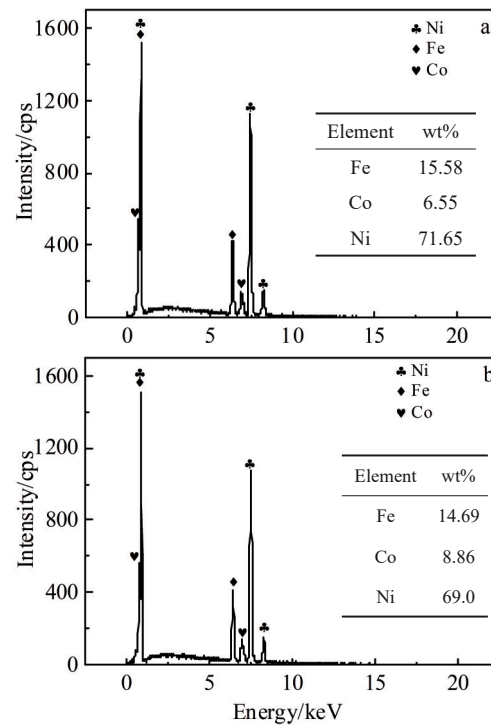


Fig.12 EDS spectra of point A (a) and point B (b) in Fig.10b

coating is used to replace the capacitive element (the dispersion index n is not equal to 1; the constant phase angle is equal to 1; the component C_{dl} is the equivalent capacitance C). Therefore, C_{dl} is the capacitance of plating/liquid double electric layer, and L is the inductance. The corresponding relationship^[28] can be expressed by Eq.(2), as follows:

$$Z(\omega) = \frac{1}{Y(j\omega)^n} \tag{2}$$

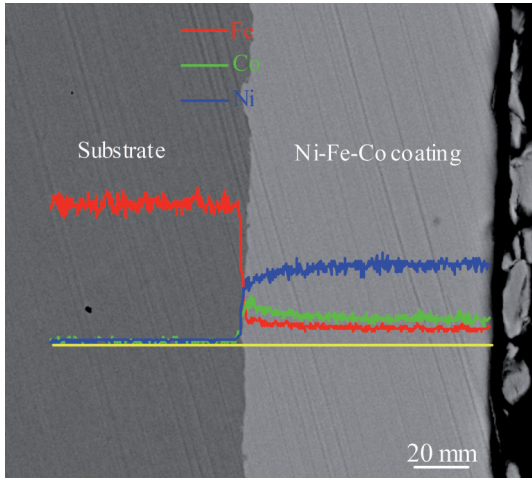


Fig.13 SEM cross-section morphology with EDS line scanning results of Ni-Fe-18.67Co coating on mild steel substrate

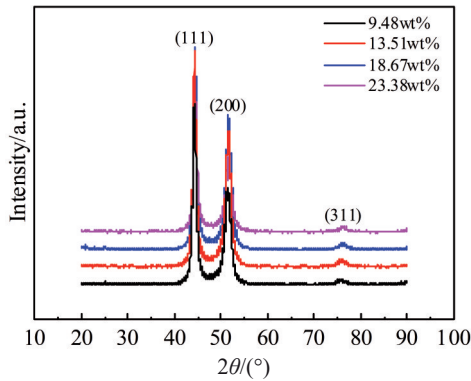


Fig.14 XRD spectra of Ni-Fe-Co alloy coatings with different Co contents

Table 1 Microhardness of different Ni-Fe-Co alloy coatings

Co content/wt%	0	9.48	13.51	18.67	23.38
Microhardness, HV/MPa	5585.0	6106.4	6142.6	6908.0	6390.6

where Z is the parameter, Y represents the admittance form of C , n is the dispersion index ($0 < n < 1$), j is the imaginary number ($j = \sqrt{-1}$), and ω is the angular frequency.

The fitting electrochemical parameters are shown in Table 2. With increasing the cobalt content, the deposited coating resistance R_f is increased firstly and then decreased. The maximum R_{ct} of Ni-Fe-Co alloy coating is $3031 \Omega \cdot \text{cm}^2$ when the Co content is 13.51wt%, i. e., the Ni-Fe-Co alloy coating with 13.51wt% Co has the optimal corrosion resistance.

The potentiodynamic polarization curves of the Ni-Fe-Co alloy coatings with different cobalt contents are shown in Fig.17a. The Tafel fitting was also conducted, and the fitting results are shown in Fig.17b and Table 3. E_{corr} and I_{corr} are the self-etching potential and self-etching current density, respectively. R_{corr} is the corrosion rate. With increasing the

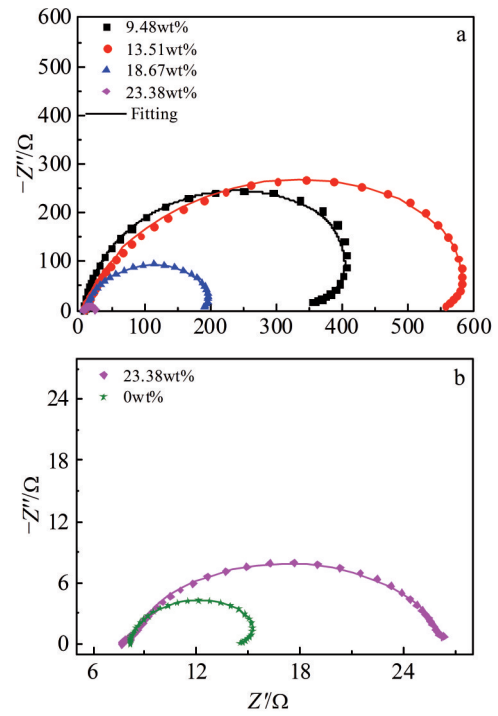


Fig.15 EIS spectra of Ni-Fe-Co alloy coatings with different cobalt contents (a); EIS spectra comparison between Ni-Fe-Co and Ni-Fe alloy coatings (b)

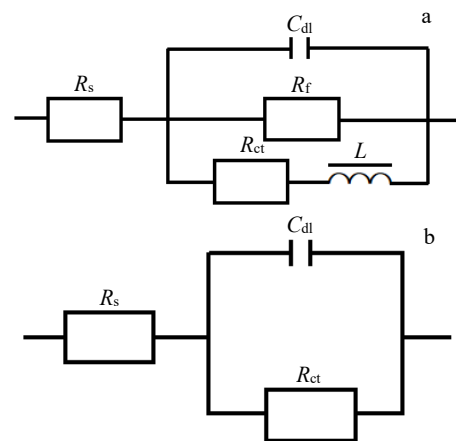


Fig.16 Equivalent circuits of Ni-Fe-Co alloy coatings with 0wt%–18.67wt% Co (a) and 23.38wt% Co (b)

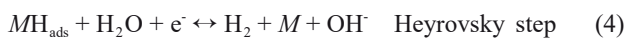
cobalt content in the alloy coating, the corrosion potential firstly shifts positively and then shifts negatively; the corrosion current is decreased firstly and then increased; the corrosion resistance firstly becomes strong and then becomes weak. Among all the alloy coatings, the Ni-Fe-Co alloy coating with 13.51wt% Co has the optimal corrosion resistance. With further increasing the Co content, the corrosion resistance is degraded, which is consistent with EIS results.

The kinetics and mechanism of hydrogen evolution reaction (HER) on the electrodes were investigated through the Tafel

Table 2 Fitting parameters of equivalent circuit of Ni-Fe-Co alloy coatings with different Co contents

Co content/wt%	Inductance, $L/H \cdot cm^2$	Solution resistance, $R_s/\Omega \cdot cm^2$	Capacitance, C_{dl}		Coating resistance, $R_f/\Omega \cdot cm^2$	Charge transfer resistance, $R_{ct}/\Omega \cdot cm^2$
			$Y_{dl}/\Omega \cdot cm^{-2} \cdot s^{-n}$	n_{dl}		
0	2.2	3.947	1.35×10^{-2}	0.91	13	9
9.48	7.3	7.72	8.11×10^{-6}	0.92	713	793
13.51	1962.2	8.31	7.23×10^{-5}	0.85	716	3031
18.67	34.7	8.46	6.73×10^{-5}	0.87	246	227
23.38	-	8.27	9.59×10^{-5}	0.91	-	18

plots and potentiodynamic polarization curves. It is generally accepted that HER in alkaline environment is firstly initiated by the electroabsorption proton discharge (Volmer step), then triggered by the electrodesorption step (Heyrovsky step) or the chemical-desorption step (Tafel step) [29]. The related mechanisms can be expressed by Eq.(3–5), as follows:



The Tafel slope is widely used to determine the main mechanism of HER, which is either in the form of Volmer-

Table 3 Fitted results of Tafel plots of Ni-Fe-Co alloy coatings with different Co contents

Co content/wt%	Corrosion potential, E_{corr}/V	Corrosion current density, $I_{corr}/A \cdot cm^{-2}$	Corrosion rate, $R_{corr}/mm \cdot a^{-1}$
0	-1.146	4.368×10^{-5}	0.5111
9.48	-1.085	1.755×10^{-5}	0.2054
13.51	-0.896	5.754×10^{-6}	0.0673
18.67	-0.948	1.778×10^{-5}	0.2081
23.38	-1.036	2.535×10^{-5}	0.2966

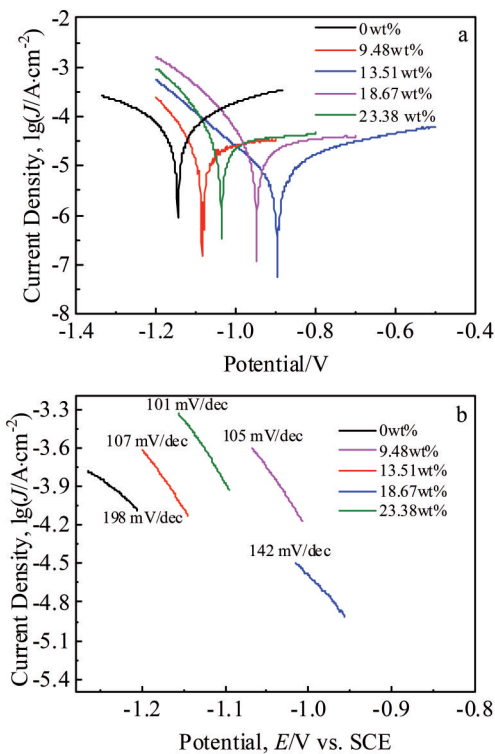


Fig.17 Potentiodynamic polarization curves (a) and Tafel plots (b) of Ni-Fe-Co alloy coatings immersed in 3.5wt% NaCl solution

Heyrovsky or Volmer-Tafel type in alkaline solution. According to the classical theory, if the Volmer step is the dominant reaction, the slope of the Tafel curve should be 120 mV/dec; if the Heyrovsky and Tafel reactions are dominant reactions, the Tafel curve slope should be 40 and 30 mV/dec, respectively. In this research, the Tafel slope of the Ni-Fe-Co alloy coatings with 0wt%, 9.48wt%, 13.51wt%, 18.67wt%, and 23.38wt% Co is 198, 107, 142, 105, and 101 mV/dec, respectively [30]. This result indicates that the Volmer step controls the overall kinetics of the reaction. The deviation from the theoretical value can be ascribed to the generation of thin surface oxide layers on the electrode surface.

Fig.18 shows the corrosion morphologies of different Ni-Fe-Co alloy coatings after electrochemical corrosion in 3.5wt% NaCl solution. The Ni-Fe-Co alloy coating with 13.51wt% Co is hardly subjected to corrosion, indicating the excellent corrosion resistance. A few black spots can be observed on the surface of the Ni-Fe-Co alloy coating with 9.48wt% Co. The surface of Ni-Fe alloy coating is severely corroded. Obvious corrosion pits appear on the surface of Ni-Fe-Co alloy coating with 18.67wt% Co. The surface of the Ni-Fe-Co alloy coating with 23.38wt% Co is loose and porous. These phenomena all indicate that the corrosive pitting occurs during the immersion in 3.5wt% NaCl solution.

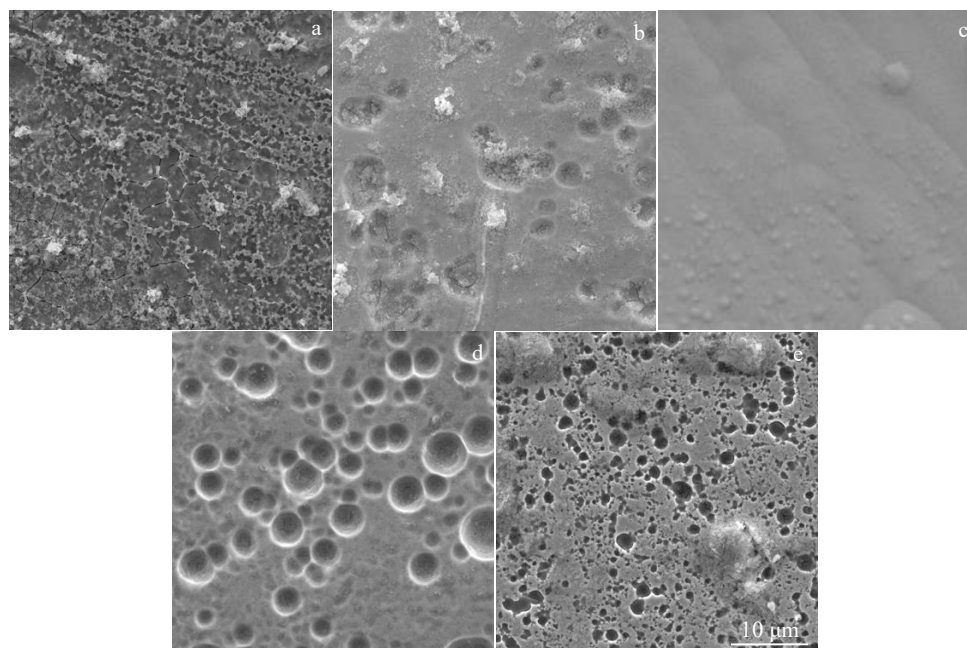


Fig.18 Corrosion morphologies of Ni-Fe-Co alloy coatings with different Co contents: (a) 0wt%, (b) 9.48wt%, (c) 13.51wt%, (d) 18.67wt%, and (e) 23.38wt%

3 Conclusions

1) The cobalt content of Ni-Fe-Co alloy coatings is increased and then decreased with increasing the current density. The cobalt content reaches a peak value at current density of 8 A/dm². The cobalt content of Ni-Fe-Co alloy coatings is increased and then decreased with increasing the electrodeposition temperature. The cobalt content reaches a peak value when the electrodeposition temperature is 45 °C. The cobalt content of Ni-Fe-Co alloy coatings is decreased and then increased with increasing the triammonium citrate content. The maximum cobalt content is obtained at triammonium citrate of 20 g/L.

2) By controlling the content of cobalt sulfate in the electroplating solution, Ni-Fe-Co alloy coatings with different cobalt contents can be obtained. The cobalt content in the coatings has a linear relationship with the cobalt sulfate content in the baths. The Ni-Fe-Co alloy coating has face-centered cubic solid solution crystal structure, and the surface brightness of the Ni-Fe-Co alloy coating is better than that of the pure nickel coating.

3) Ni-Fe-Co alloy coatings have high microhardness with 9.48wt% – 23.38wt% Co. The maximum microhardness is 6908.0 MPa when the Co content is 18.67wt%. The optimal corrosion resistance of Ni-Fe-Co alloy coating is achieved when the cobalt content is 13.51wt%. When the cobalt content exceeds 13.51wt%, the corrosion resistance becomes worse, and the corrosion mechanism is pitting corrosion.

References

- Cai F, Jiang C H, Zhang Z Q et al. *Journal of Alloys and Compounds*[J], 2015, 635: 73
- Zhang W W, Du S S, Li B S et al. *Journal of Alloys and Compounds*[J], 2021, 865: 158 722
- Jin Guo, Ding Xiaolong, Hu Zhenfeng et al. *Rare Metal Materials and Engineering*[J], 2019, 48(6): 2002 (in Chinese)
- Shi Yangyang, Cheng Guanggui. *Rare Metal Materials and Engineering*[J], 2016, 45(4): 952 (in Chinese)
- Gui M C, Kang S B. *Metallurgical and Materials Transactions A*[J], 2001, 32(9): 2383
- Safavi M S, Etmnanfar M. *Journal of Ultrafine Grained and Nanostructured Materials*[J], 2019, 52(1): 1
- Harimkar S P, Bakshi S R, Agarwal A. *JOM*[J], 2013, 65(6): 739
- Abdoos M, Amadeh A A, Adabi M. *Transactions of the Institute of Metal Finishing*[J], 2019, 97(3): 146
- Shi L, Sun C F, Zhou F et al. *Materials Science and Engineering A*[J], 2005, 397(1–2): 190
- Jana R, Pathak T P, Sigman M S. *Chemical Reviews*[J], 2011, 111(3): 1417
- Jing P P, Liu M T, Pu Y P et al. *Scientific Reports*[J], 2016, 6(1): 37 701
- Vicenzo A. *Journal of the Electrochemical Society*[J], 2013, 160(11): D570
- Torabinejad V, Aliofkhaezrai M, Assareh S et al. *Journal of Alloys and Compounds*[J], 2017, 691: 841
- Suryanto B H R, Wang Y, Hocking R K et al. *Nature Communications*[J], 2019, 10(1): 5599
- Chen J D, Zheng F, Zhang S J et al. *ACS Catalysis*[J], 2018, 8(12): 11 342
- Hu X, Hval H H, Bjerglund E T et al. *ACS Catalysis*[J], 2018, 8(7): 6255
- Yang H, Li X J, Zhou H et al. *Journal of Alloys and Compounds*

- [J], 2011, 509(4): 1217
- 18 Lee C H, Bonevich J E, Davies J E et al. *Journal Electrochemical Society*[J], 2008, 155(7): D499
- 19 Petegem S V, Zimmermann J, Brandstetter S et al. *Acta Materialia*[J], 2013, 61(15): 5835
- 20 Lee T R, Chang L W, Chen C. *Surface and Coatings Technology*[J], 2012, 207: 523
- 21 Li Y Q, Cai X F, Zhang G Q et al. *Journal of Alloys and Compounds*[J], 2022, 903: 163 761
- 22 Geng S J, Qi S J, Xiang D et al. *Journal of Power Sources*[J], 2012, 215: 274
- 23 Zhou J T, Hu X W, Li J L et al. *International Journal Hydrogen Energy*[J], 2021, 46(79): 39 457
- 24 Liu X M, Zangari G, Shen L Y. *Journal of Applied Physics*[J], 200, 87(9): 5410
- 25 Bard A J, Faulkner L R. *Russian Journal of Electrochemistry*[J], 2002, 38(12): 1364
- 26 Pour Z S, Ghaemy M, Bordbar S et al. *Progress Organic Coatings*[J], 2018, 119: 99
- 27 Sanaty-Zadeh A, Raeissi K, Saidi A et al. *Journal of Alloys and Compounds*[J], 2009, 485(1-2): 402
- 28 Jorcin J B, Orazem M E, Pébère N et al. *Electrochimica Acta*[J], 2006, 51(8-9): 1473
- 29 Wu L, He Y H, Lei T et al. *Energy*[J], 2014, 67: 19
- 30 Rosalbino F, Delsante S, Borzone G et al. *International Journal of Hydrogen Energy*[J], 2008, 33(22): 6696

电沉积 Ni-Fe-Co 合金镀层的微观结构及耐腐蚀性能

彭昭玮^{1,2,3}, 李伟洲^{1,3}, 彭成章⁴

(1. 广西大学 资源环境与材料学院, 广西 南宁 530004)

(2. 广西大学 化学化工学院, 广西 南宁 530004)

(3. 广西大学 广西有色金属及特色材料加工重点实验室, 广西 南宁 530004)

(4. 湖南科技大学 机电工程学院, 湖南 湘潭 411201)

摘要: 在稳定的酸性柠檬酸盐溶液中, 在低碳钢基体上电镀获得了 Ni-Fe-Co 合金镀层, 并研究了电镀条件和钴含量对镀层性能的影响, 得到了最佳镀层工艺参数。利用扫描电子显微镜、能谱仪、电化学阻抗谱、极化曲线和数字显微硬度计对合金镀层进行了研究。结果显示, 合适的工艺参数是 10 A/dm²、45 °C 和 10 g/L 柠檬酸三铵。Ni-Fe-Co 合金镀层的钴含量随着钴离子浓度的增加而线性增加, 镀层均为简单的面心立方固溶体结构。随着镀层中钴含量的增加, 镀层的耐腐蚀性能和硬度先升高后降低。Ni-Fe-13.51Co (质量分数) 镀层具有显著的防腐蚀性能, 其电荷转移电阻为 3031 Ω·cm², 腐蚀电流密度为 5.754×10⁻⁶ A/cm²。

关键词: 电沉积; Ni-Fe-Co 合金镀层; 显微硬度; 腐蚀

作者简介: 彭昭玮, 男, 1995年生, 博士生, 广西大学资源环境与材料学院, 广西 南宁 530004, E-mail: pengzhaowei_gxd@163.com